ELSEVIER

Contents lists available at ScienceDirect

Electrochimica Acta

journal homepage: www.elsevier.com/locate/electacta



Detecting Potassium Ion Gradients at a Model Graphitic Interface



Zachary J. Barton^a, Jingshu Hui^{a,b}, Noah B. Schorr^a, Joaquín Rodríguez-López^{a,*}

- a Department of Chemistry, University of Illinois at Urbana-Champaign, 600 South Mathews Avenue, Urbana, Illinois 61801, United States
- b Department of Materials Science and Engineering, University of Illinois at Urbana-Champaign, 1304 West Green Street, Urbana, Illinois 61801, United States

ARTICLE INFO

Article history: Received 22 February 2017 Received in revised form 17 April 2017 Accepted 20 April 2017 Available online 21 April 2017

Keywords:
Alkali Ion Intercalation
Mercury Electrode
Potassium Ion Battery
Scanning Electrochemical Microscopy
(SECM)

ABSTRACT

Potassium ion batteries (KIBs) are gaining attention as attractive, low-cost alternatives to lithium ion batteries (LIBs). Emerging KIB materials are not yet fully understood, so *in situ* characterization techniques are being developed to address the similarities and differences to the operation of LIB materials, including aspects of interfacial ion transfer and solid electrolyte interphase (SEI) formation. Here, we introduce the use of Hg disc-well microelectrodes as probes in scanning electrochemical microscopy (SECM) for the detection of K⁺ gradients on an operating graphitic material. Electrochemically controlled amalgamation and stripping reactions on these probes permit their accurate positioning near a conductive surface, and the detection of local concentration changes once the substrate is biased to intercalate K⁺. K⁺ reduction into the Hg phase follows a behavior similar to that of Li⁺ and Na⁺ and yields an electrochemical response that is used to evaluate local substrate reactivity. Using these probes *in situ*, we demonstrate the reversible intercalation of K⁺ on a surface site of patterned highly oriented pyrolytic graphite (HOPG), a model interface for carbonaceous KIB materials. Our method affords a direct measurement of localized K⁺ fluxes, which are not resolvable through bulk electroanalytical techniques, thus making our approach potentially informative about reaction mechanisms for nascent KIB-based energy storage technologies.

© 2017 Elsevier Ltd. All rights reserved.

1. Introduction

The field of portable energy storage is dominated by Li+ batteries (LIBs), which operate by the reversible insertion and extraction of Li⁺ at anode and cathode host materials [1]. Though LIBs meet present portable energy storage needs, the rising cost and material shortage of lithium sources pose challenges to the long-term sustainability of LIB technologies [2,3]. K-ion batteries (KIBs) are an attractive alternative to LIBs since potassium is ~1000 times more abundant than lithium in the Earth's crust [4,5]. In addition, the theoretical voltage limits for KIBs and LIBs are similar $(-2.925 \text{ V vs. NHE for K/K}^+ \text{ and } -3.045 \text{ V vs. NHE for Li/Li}^+)$ [6], so sustained technological developments may be able to bring commercially competitive KIBs to the market. Preliminary studies suggest that carbonaceous materials such as hard carbon [7], graphite [8-10], graphene oxide [10], and nitrogen-doped graphene [11] may be good candidates for a KIB anode. Diversifying the materials pool for high performance energy storage requires a deeper understanding of the similarities and differences between LIBs and emerging ion insertion technologies. Building on our previous investigations of interfacial Li * fluxes [12] and ionic staging mechanisms in multi-layer graphene [13], here we turn our attention to K^* fluxes.

Scanned probe methods are often employed for surface investigations at energy storage materials, but few methods of in situ chemical imaging of ionic reactions at the batteryelectrolyte interface exist [14-17]. Recently, we reported the use of Hg-based scanning electrochemical microscopy (SECM) probes for the detection of alkali ions via anodic stripping voltammetry [18]. In this technique, the reduction of the metal ion and subsequent diffusion of the metal into the Hg phase creates a steady-state amalgamation current, which upon reversal of the potential scan direction yields a stripping peak. Both of these signals can be used for quantitative detection of differences in the local concentrations of various ions as a function of electrode activation, as well as for accurate positioning of the SECM probe. Furthermore, we recently reported the fabrication and stripping voltammetry of Hg disc-wells, which consist of a level pool of Hg confined to the glass-walled cavity before a recessed Pt microdisc [19–21]. These probes demonstrated their superior performance as SECM probes for the detection of Li⁺ and Na⁺, as compared to traditional Hg sphere-caps. The K+/K(Hg) redox pair shares similar

Corresponding author.
 E-mail address: joaquinr@illinois.edu (J. Rodríguez-López).

electrochemical attributes with Li⁺/Li(Hg) and Na⁺/Na(Hg), so the same types of probes are able to detect this species [22-24]. Due to their chemical and mechanical robustness as well as their unique ability to directly access ion-specific information, Hg disc-wells enable SECM to pursue answers connecting chemical structures to their electrochemical performance in systems involving ionic gradients. Here, we demonstrate the measurement of ionic gradients on a model material for a KIB anode-highly oriented pyrolytic graphite (HOPG). While insertion of K⁺ on this material is not ideal, the detection of ionic gradients over surface features upon activation is accurately tracked, independently from the activity measured at the substrate electrode. The application of SECM techniques for the chemical measurement of ion fluxes at KIB electrodes will enable further understanding of the impact of solid-electrolyte interphase (SEI) formation and electrode structure on the reactivity of emerging materials.

2. Experimental

2.1. Chemicals and Supplies

All chemicals were purchased as A.C.S. reagent grade or better and used as received without further purification. Nitric acid and water (ChromAr grade) were obtained from Avantor. Platinum wire (25 μm and 0.5 mm diameter) and silver wire (1 mm diameter) were obtained from Goodfellow. Ethylene carbonate (EC, anhydrous, 99%), mercury(II) nitrate monohydrate ($\geq 99.99\%$ trace metals basis), potassium hexafluorophosphate (99.5%), propylene carbonate (PC, anhydrous, 99.7%), tetrabutylammonium hexafluorophosphate (NBu₄PF₆, 99.0%) and N,N,N',N'-tetramethyl-p-phenylenediamine (TMPD, 99%) were obtained from Sigma-Aldrich. Tetramethylammonium nitrate (NMe₄NO₃) was obtained from Southwestern Analytical Chemicals.

Highly ordered pyrolytic graphic (HOPG, brand grade SPI-2) was purchased from SPI supplies. 3MTM copper conductive tape with a single conductive glue adhesive surface was purchased from Ted Pella, Inc. Microposit S1813 photoresist was purchased from

MicroChem. AZ 917 MIF developer was purchased from AZ Electronic Materials. Ultra high purity (UHP) argon was obtained from Airgas.

2.2. Hg Disc-Well Electrode Fabrication

Hg disc-well probes were fabricated by etching Pt disc ultramicroelectrodes (UMEs), electrodepositing Hg in the cavity, and removing excess Hg with a flexible glass coverslip as previously published [21]. Specifically, Pt UMEs with a Pt radius (a_1) of 12.5 μ m and a glass ratio $(R_G = a_2/a_1, a_2 = \text{total probe radius})$ smaller than 4 were etched in a solution of 30 v. % sat. CaCl₂ + 10 v. % HCl in H₂O for 40 s under ultrasonic agitation while applying a peak-to-peak voltage (V_{p-p}) of 2.70V at 60 Hz with a variac. This gave an etched cylindrical cavity with a normalized depth $(H_2 = h_2)$ a_1 , h_2 = depth of cavity) of 1.1. Hg was deposited potentiostatically at $+0.2 \text{ V vs. Ag/AgCl in } 20 \text{ mM Hg}(NO_3)_2 \cdot H_2O + 0.2 \text{ M NMe}_4NO_3 \text{ and}$ 0.5 v. % HNO₃ in H₂O until the deposition current reached 0.3 µA. indicating the growth of a Hg sphere-cap protruding from the overfilled cavity. The Hg deposit was then leveled and rinsed with H₂O to remove displaced Hg droplets, resulting in a Hg disc-well with a flat, mirror-like surface having a normalized height $(H_1 = h_1)$ a_1 , h_1 = Hg sphere-cap height) of 0 (Fig. 1).

2.3. Substrate Fabrication and Patterning

Cu tape was used to mechanically exfoliate thin HOPG samples from a larger HOPG block. Following our previously published graphene patterning method [13], the thin HOPG samples were treated with photolithography to create patterned windows to expose selected areas of the HOPG surface using a mask. The exposed HOPG was then etched by a Plasma Lab Freon/O2 reactive ion etching (RIE) system with 37 mW RF energy under a pressure of 40 mTorr while flowing 20 sccm O2 for 1 min. After RIE, the remaining photoresist was removed by rinsing with acetone and isopropanol. The resulting regular array of holes measured $\sim\!\!43\,\mu m$ wide and $\sim\!\!1.4\,\mu m$ deep (Figure A1). Neighboring holes were separated by 500 μm , measured from their centers.

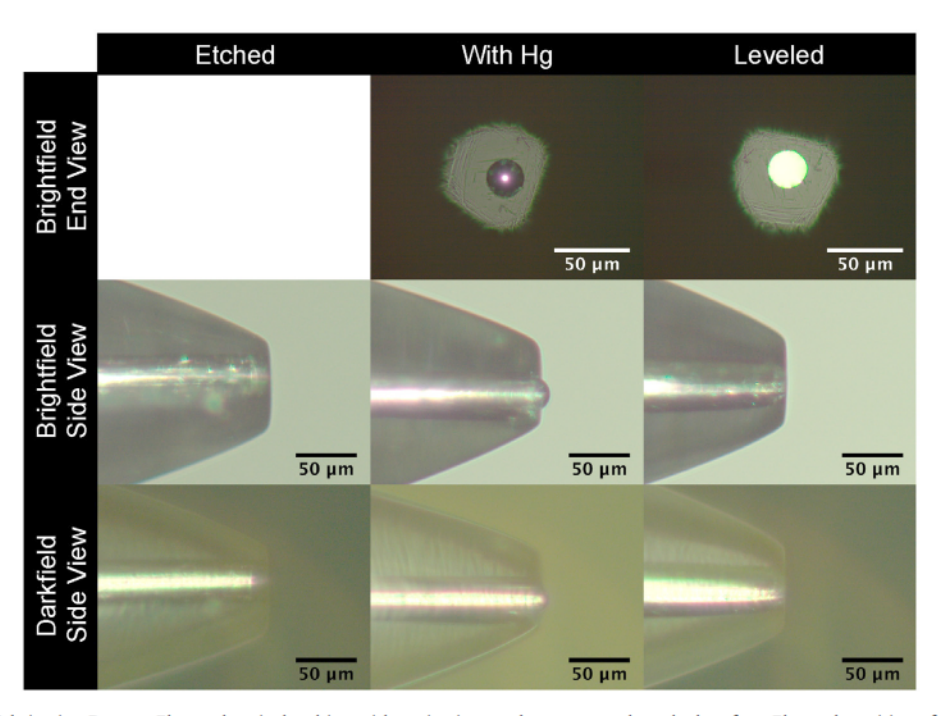


Fig. 1. Hg Disc-Well Probe Fabrication Process. Electrochemical etching with sonication produces an evenly etched surface. Electrodeposition of Hg is terminated after overfilling the etched cavity. After leveling, the Hg disc-well is evenly filled and has a flat, mirror-like surface. The Hg disc-well shown here has $a_1 = 12.5 \mu m$, $R_G = 2.5$, $H_1 = 0$, and $H_2 = 1.1$.

2.4. Ex Situ Optical and Spectroscopic Measurements

Hg disc-well probe dimensions were verified though optical microscopy (Zeiss AxioLab.A1). In addition to optical microscopy, HOPG samples were characterized through scanning electron microscopy (SEM, Hitachi S-4800 high resolution SEM), Raman spectroscopy and imaging (Nanophoton Laser Raman Microscope RAMAN-11) (Fig. 2).

2.5. Electrochemical Experiments

All electrochemical measurements were performed with a CHI 920D SECM under oxygen- and water-free conditions in an MBRAUN UniLab glovebox filled with UHP argon. All solutions were made in a PC and EC solvent mixture with 1:1 ratio (vol./vol.), which is hereafter referred to as PC-EC. The Teflon SECM cell was fitted with a patterned HOPG substrate (19.6 mm²), a Pt wire counter electrode (CE), and a Ag wire quasi-reference electrode (QRE). Substrate CVs and CV-SECM used a Ag/Ag⁺ (0.1 M AgNO₃ in PC-EC) reference electrode (RE) instead of the Ag QRE to poise the cell potential. Potentials referenced against a 0.1 M Ag/Ag⁺ RE (3.604 V vs. 0.1 M K/K⁺) are reported vs. 0.1 M K/K⁺ for clarity.

Prior to SECM investigations, the patterned HOPG electrode was cycled in 0.1 M KPF₆ in PC-EC for 6 cycles between 0.604 to 0.004V vs. 0.1 M K/K⁺ at 1 mV s⁻¹ to form a stable SEI layer. In order to better observe K⁺ intercalation and deintercalation processes, additional CVs with HOPG were acquired at 50 μ V s⁻¹ in 1 mM KPF₆ in PC-EC after SECM experiments (Fig. 3).

A Hg disc-well UME performing TMPD oxidation in a solution of 2 mM TMPD and 0.1 M KPF₆ in PC-EC was used to collect an SECM feedback image (Fig. 4) to find the approximate locations of etched holes. To avoid interference from oxidized TMPD generated at the CE, the cell was rinsed with PC and refilled with 1 mM KPF₆ in PC-EC. The Ag QRE was also swapped for a Ag/Ag⁺ RE after the removal of TMPD from the cell. The same Hg disc-well probe was then approached to the substrate with a cyclic voltammetry probe scan surface (CV-PSS) in the Z direction (Fig. 5). After reaching the HOPG surface, the probe was positioned directly over an etched hole and used to record a series of CVs with regular sequential incrementing (and then decrementing) of the substrate potential.

3. Results and Discussion

3.1. Ex Situ Optical and Spectroscopic Measurements

An SEM image of patterned HOPG shows a regular array of holes measuring ${\sim}43~\mu m$ in diameter and separated from their nearest neighbors by 500 μm (Fig. 2A). The holes' size and center-to-center distance match with the designed pattern.

Raman spectra (Fig. 2B) show the clear presence of a D band for etched holes but not for pristine HOPG. The D band corresponds to carbon ring "breathing" modes and is indicative of structural disorder, such as exposed graphitic edge planes [25]. In LIBs, uptake of Li⁺ is greater at graphitic edge planes than at the basal plane [26], so we expected to find similar ionic activity for K⁺ in the present system. Following electrochemical cycling and SECM

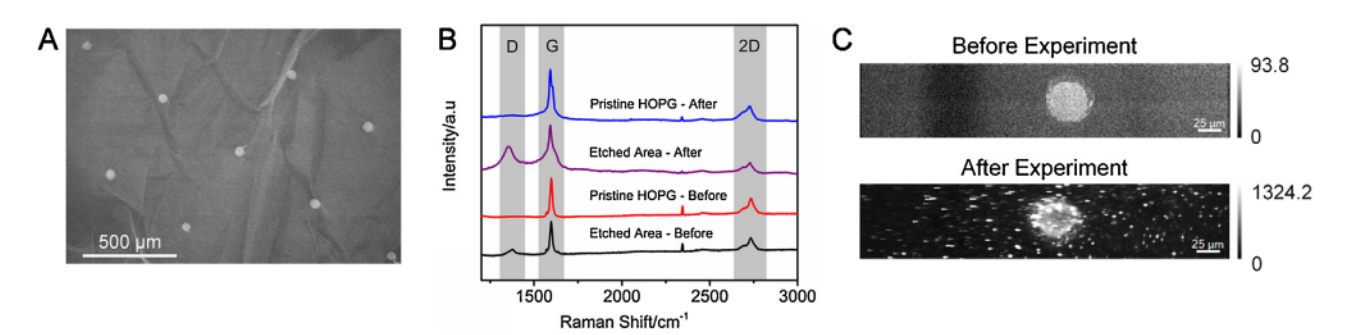


Fig. 2. SEM and Raman Characterization of Patterned HOPG. (A) An SEM image shows the pattern etched holes on HOPG. The holes are ~43 μm wide, ~1.4 μm deep, and 500 μm from their nearest neighbors, measured from their centers. (B) Raman spectra before and after electrochemical experiments exhibit a D band signal only over the etched holes. (C) Raman mapping of the D band intensity before and after electrochemical experimentation shows an increase in D band signal limited to the etched holes.

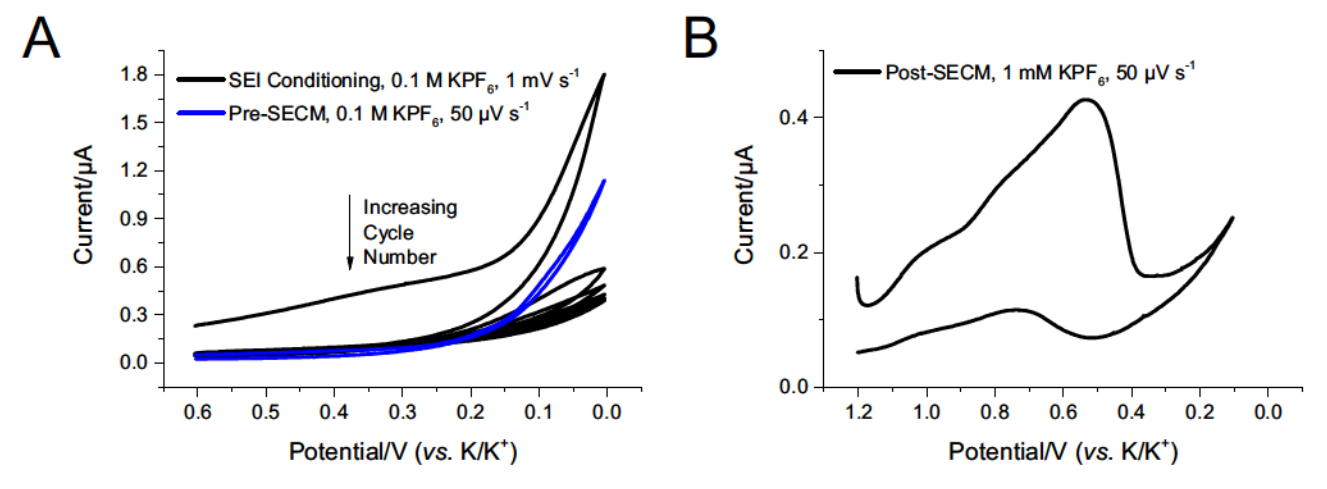


Fig. 3. Cyclic Voltammetry of K^* Intercalation and Deintercalation at Patterned HOPG. (A) Initially observed broad, irreversible peaks diminished with cycling number, eventually resulting in a clean, stable background signal. (B) After forming the SEI, a K-ion de-intercalation process was observed at 0.52V (vs. K/ K^*).

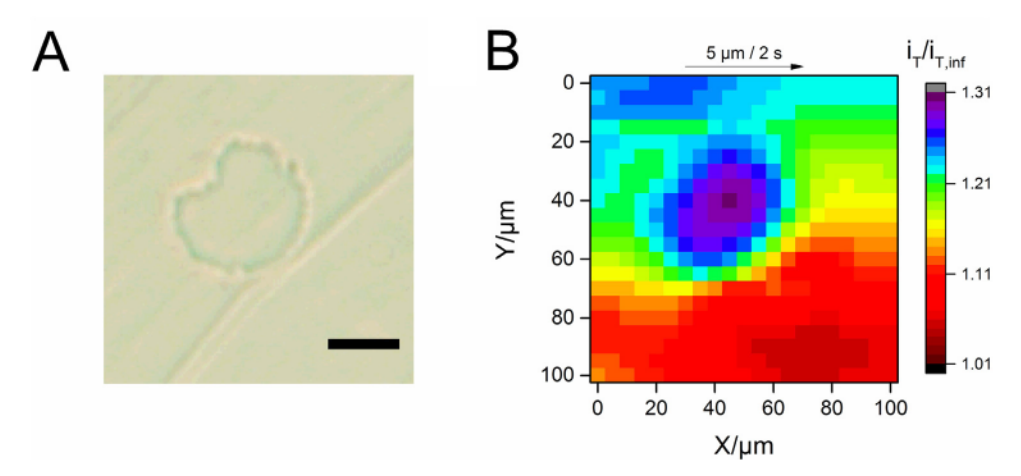


Fig. 4. Identification of Etched Hole. (A) Optical micrograph of an etched hole in HOPG. The scale bar represents 25 μ m. (B) SECM feedback image of the region shown in A taken with a Hg disc-well in 2 mM TMPD+0.1 M KPF₆ in PC-EC.

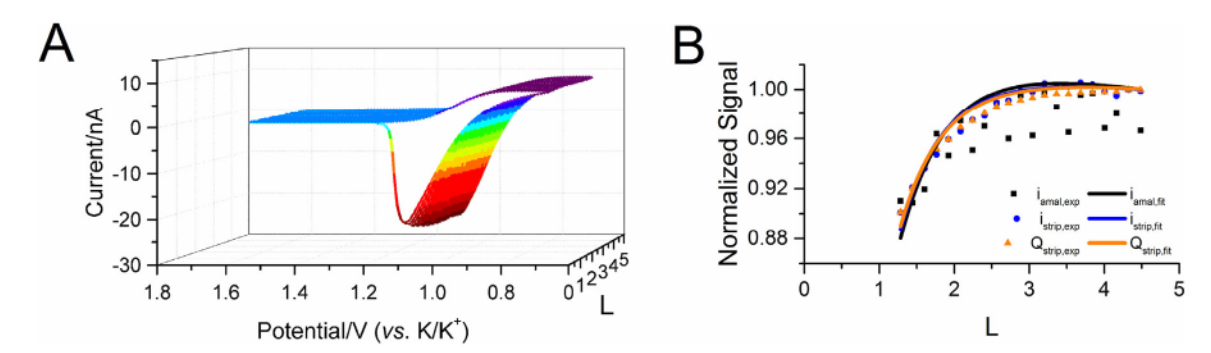


Fig. 5. CV-SECM Stripping-Based Approach. (A) CV-PAS based on $K^* + e^- \rightleftharpoons K(Hg)$ ending with $L = 1.28 \pm 0.02$ at $[X, Y] = [0 \ \mu m, 0 \ \mu m]$ in Fig. 4B. (B) Extracted CV-PACs and fits based on COMSOL simulations. Key simulation conditions include: $a_1 = 12.5 \ \mu m, R_G = 2.5, H_1 = 0, H_2 = 1.1, C_{ox}^* = 1 \ mol \ m^{-3}, D_{K*,PC-EC} = 2 \times 10^{-10} \ m^2 \ s^{-1}, and D_{K(Hg), Hg} = 7.9 \times 10^{-10} \ m^2 \ s^{-1}, \Delta E = 0.295 \ V, \nu = 0.2 \ V \ s^{-1}, \alpha = 0.5, and <math>k^0 = 1 \times 10^{-2} \ m \ s^{-1}.$

experiments, the D band remained nearly unchanged over unetched areas but showed a marked increase over etched holes (Fig. 2B). The increase in D band intensity is consistent with the evolution of structural disorder expected from the repeated K⁺ insertion and extraction. The localization of this increase in D band intensity to the etched holes (Fig. 2C) suggests that exposed edge planes serve as primary sites for potassium ion intercalation.

3.2. Substrate Cycling and SEI Formation

The HOPG substrate was first cycled at 1 mV s $^{-1}$ in 0.1 M KPF₆ in PC-EC for 6 cycles to form a stable SEI layer. Initial cycles showed broad, irreversible peaks that are likely attributable to solvent and electrolyte decomposition processes, such as those found in LIB systems (Fig. 3A) [13,27,28]. The intensity of these peaks diminished with cycling, eventually resulting in a clean background signal. Following SEI formation, cycling more slowly at $50~\mu V s^{-1}$ allowed the identification of K⁺ intercalation behavior at $E < 0.54 V~(vs. K/K^+)$, in addition to various unknown processes from $\sim 1.10~V$ to $0.54~V~(vs. K/K^+)$, and a de-intercalation event at $0.52~V~(vs. K/K^+)$ on the return sweep (Fig. 3B).

3.3. Identification of Region of Interest

A Hg disc-well UME (a_1 = 12.5 μ m, R_G = 2.5) was positioned approximately one probe radius (L = $d/a_1 \sim 1$, d = tip-substrate gap) above the HOPG surface through a probe scan curve (PSC) in the Z direction using TMPD as the redox mediator and with the substrate left at open circuit. After rapidly imaging a large area to identify a

region of interest (Fig. A2), an area containing a single etched hole (Fig. 4A) was slowly imaged at 2.5 μ m s⁻¹ (Fig. 4B). This speed was selected to prevent distortions based on forced convective transport [29]. Initial SECM images exhibited negative feedback consistent with the insulating nature of SEIs observed for other alkali ions [13]. However, over time we observed a shift towards partial positive feedback. We believe this could be a result of some SEI degradation process or the incorporation of TMPD in the SEI. Though positive feedback is observed at all points in the image, even greater positive feedback occurs over the etched hole centered at $[X, Y] = [45 \mu m, 45 \mu m]$. If the reactivity of the holes and the basal plane were equal, the SECM feedback current observed over holes would be less than over the basal plane due to the increased tip-substrate gap over holes. The possibility of electron transfer at the HOPG basal plane [30], the susceptibility of HOPG to adventitious contaminants [31], and the large number of exposed edge sites on this sample do not allow a straightforward quantification of the contributions from basal and edge planes. However, the observed increase in feedback current over the etched hole is supported by Raman spectra (Fig. 2B), which suggest far greater planar disorder in the etched holes in comparison to the pristine basal plane, and is consistent with the increased electrochemical activity observed at electronic structure distortion sites in carbonaceous materials, such as graphene [32-35].

3.4. Stripping-Based Approach to HOPG

After switching to a 1 mM KPF₆ solution in PC-EC, the Hg discwell UME was re-approached to the origin in Fig. 4 by recording stripping CVs between Z motor increments (Fig. 5) with the HOPG left unbiased at its open circuit potential. Because ions are regularly stripped from the Hg probe, this method of approaching a surface avoids the risk of damaging the Hg probe by saturation of the amalgam phase. The amalgamation current (iamal), peak stripping current (i_{strip}), and stripping charge (Q_{strip}) were each extracted from the CV-PAS dataset to give three CV-PACs [18]. Of these, Q_{strip} exhibited the least noise, which is consistent with the general insensitivity of integrated values to temporal fluctuations in a source signal. The negative feedback stripping charge CV-PAC was fit with an analytical model derived from COMSOL finiteelement simulations [21] to obtain the final approach distance of $L = 1.28 \pm 0.02 \ (\chi_{red}^2 = 4.0401 \times 10^{-5})$. Though smaller gaps are possible, wrinkles in the HOPG surface (Fig. 2A) warranted caution to avoid mechanical damage to either the probe or the substrate. The final approach distance is consistent with the normalized timescale $(T_{amal} = D_{ox} \Delta E / (v^* a_1^2))$ of 1.9 \pm 0.2, for which the average Nernstian diffusion layer thickness (δ_N) is $7.7 \pm 0.1 \,\mu m$ [36]. This timescale ensures that the depletion volume expanding from the SECM probe during amalgamation propagates far enough into solution to overlap with ionic gradients emanating from the substrate. The overlap between the probe and substrate diffusion fields is the source of informational probe signal perturbations. Negative feedback was observed for all three signals due to the increasingly hindered diffusion field with decreasing tip-substrate gap. The observation of positive feedback from TMPD redox signals and negative feedback from K(Hg) amalgamation and stripping signals demonstrates one of the key benefits of Hg disc-well SECM probes, namely, that amalgamation and stripping signals allow negative feedback SECM probe positioning over any substrate regardless of the substrate's electrical conductivity [18]. Furthermore, since stripping signals afford potential-based ionic specificity, Hg-based CV-SECM signals may provide accurate measurements even in concentrated solutions that are traditionally challenging for methods lacking this specificity, such as those based on resistance, conductance, or impedance [16].

3.5. CVs with Substrate Competition

To show that Hg-based electrodes can directly probe changing ionic gradients, the Hg disc-well UME was positioned over unmodified HOPG at [X, Y] = $[0 \mu m, 45 \mu m]$ and programmed to record a series of CVs with the substrate following a sequential staircase potential sweep. Scanning the potential at $0.2 \,\mathrm{V \, s^{-1}}$ under the tested conditions gave $T_{amal} = 2.4 \pm 0.2$. As the substrate potential increased (Fig. 6A), activating K+ intercalation, all three Hg disc-well signals decreased (Fig. 6C) while the substrate current increased (Fig. 6D). Then, as the substrate potential was stepped anodically to allow K+ deintercalation (Fig. 6B), the Hg disc-well signals increased in kind as the substrate current decreased, indicating the restoration of the local K+ concentration. The total decrease in probe signal between inactive and fully active substrate potentials was 3.71 nA (56%) for i_{amal} , 17.6 nA (90%) for i_{strip} , and $3.29 \, \text{nC} (89\%) \, \text{for} \, Q_{strip}$. After testing over a pristine region of HOPG, the Hg disc-well UME was positioned directly over an etched hole at $[X, Y] = [45 \mu m, 45 \mu m]$ and made to repeat the same test sequence. As before, all three Hg disc-well signals decreased and then recovered in response to substrate activation then deactivation towards K⁺ intercalation. The total decrease in probe signal between inactive and fully active substrate potentials was 2.06 nA (30%) for i_{amal} , 17.7 nA (77%) for i_{strip} , and 3.24 nC (77%) for Q_{strip} .

We hypothesize that the probe signal discrepancies, specifically, the larger changes in i_{strip} and Q_{strip} in comparison to i_{amal} , are due to cross-talk between the probe and the substrate in this low K^+ concentration regime [37]. Such low K^+ concentrations were used in order to safely access timescales allowing good ionic

resolution and avoid saturating the ionic capacity of the thin HOPG sample but led to larger than ideal shared resistance between the two working electrodes. In the interest of avoiding co-intercalation phenomena [38–40], no additional supporting electrolyte was present. i_{strip} and Q_{strip} are typically valuable for their ionic specificity and enhanced sensitivity due to pre-concentration of the amalgam phase, but the observed potential shifts compromised their usefulness in this particular system.

Nevertheless, i_{amal} remained a reliable metric of the local K⁺ concentration since it reached a quasi-steady-state and does not depend on the accumulation of K⁺ within the Hg probe over time. In both sites explored, the relatively stable i_{amal} signal for $E_{\text{sub}} \ge 0.5 \,\text{V}$ suggests that the cathodic peaks observed in the HOPG voltammetry (Fig. 3B) are not associated with K⁺ uptake. It is reasonable to suspect that these peaks may be associated with changes in the SEI. $i_{amal}(E_{sub})$ is described well by a simple exponential function of the form $i_{amal} = A + B^* \exp(C^* E_{sub})$, where A, *B*, and *C* are freely varying constants, for both the activation $(\chi^2_{\rm red.} = 1.62 \times 10^{-20} \text{ for pristine HOPG and } \chi^2_{\rm red.} = 2.26 \times 10^{-21} \text{ for }$ etched holes) and deactivation ($\chi^2_{\rm red.} = 2.13 \times 10^{-20}$ for pristine HOPG and $\chi^2_{\rm red.} = 2.26 \times 10^{-21}$ for etched holes) substrate potential sequences (Fig. A3), which suggests that the Hg disc-well closely followed the electrochemical uptake of K+ by the substrate. Therefore, despite challenges unique to the system under study, these results demonstrate the ability of Hg disc-well SECM probes to track dynamic ionic fluxes at operating KIB interfaces.

Considering the enhanced positive feedback current in the SECM image (Fig. 4B) and the pronounced D band in the Raman spectra (Fig. 2B) over etched holes, we expected to observe a clear increase in K⁺ uptake over etched holes in comparison to pristine sites due to the greater concentration of exposed edge planes at etched sites. Contrary to expectations, a greater proportional decrease in i_{amal} was observed over the pristine HOPG than over the etched hole. However, microscopic inspection of the pristine surface does indicate a large density of steps (Fig. 4A), exposing edge sites at which the ionic flux could rival that of artificiallydefective holes. Another possible explanation for the small differences observed between the pristine and hole sites is that the SEI formed on this KIB electrode strongly controls the flux of K⁺, thus decreasing contrast between neighboring surface sites. Furthermore, the consistent i_{amal} registered at E_{sub} = 1.604 V, where the substrate is electrochemically inactive, is evidence that the bulk K⁺ concentration was not significantly affected. Despite this, the average substrate current decreased with each cycle (Figs. Fig. 66D and A4). Therefore, we conclude that the substrate's activity towards K⁺ uptake and release decreased with use and/or time. Regardless of the cause, this overall decrease in substrate activity was sufficiently large to obscure whatever differences in K+ uptake and release may have been originally present over the pristine HOPG and etched holes. The decrease in K+ uptake by the substrate with each cycle was also a contributing factor to the smaller distortions of i_{strip} and Q_{strip} when a test sequence was subsequently repeated at the same locations with a longer normalized timescale-obtained by increasing the overpotential and decreasing the potential scan rate (Fig. A4).

While the measurement of K⁺ fluxes at the activated KIB electrode–electrolyte interface was successful, this first exploration did not show significant differences in ionic uptake between two sites with different redox reactivity. Rather than a lack of contrast, the absence of meaningful differences at the two location types actually demonstrates the sensitivity of Hg disc-wells to local ionic fluxes, which can distinguish between various degrees of substrate uptake of a particular ionic species *in situ*. The probes accurately reported the changing ionic fluxes, but differences in K⁺ uptake over pristine and etched regions were overwhelmed by the much larger impact of substrate aging. While HOPG is certainly not

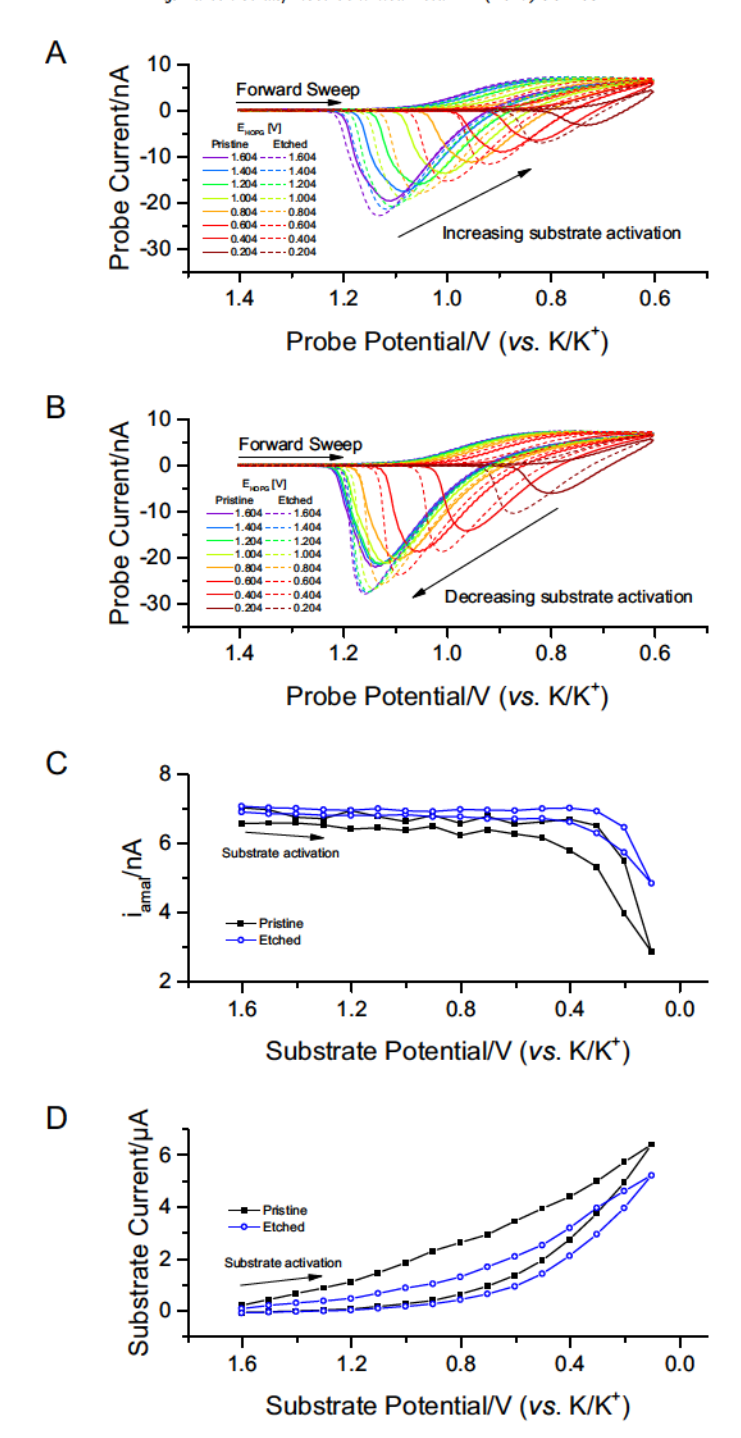


Fig. 6. Competition for K* over Etched Hole. (A) Select Hg disc-well CVs taken with increasing substrate activation towards K* intercalation. ν = 0.2 Vs $^{-1}$, T_{amat} = 2.4 ± 0.2, δ_N = 7.9 ± 0.1, and w_N = 0.633 ± 0.007. (B) Select Hg disc-well CVs taken with decreasing substrate activation, giving way to K* deintercalation. (C) Hg disc-well amalgamation currents extracted from A and B. (D) Average chronoamperometric signal at the substrate at various activation potentials.

an ideal electrode material under the tested conditions, the methodology shown here might be useful to distinguish the different K⁺-consuming processes that underlie the complex response observed on KIB electrodes.

4. Conclusions

We have used a novel electrochemical probe to obtain direct measurements of K^+ uptake by a representative graphitic anode material for KIBs. Our SECM investigations with a Hg disc-well UME revealed increased electronic conductivity as well as

reversible K^+ intercalation and deintercalation over exposed HOPG edge planes. When positioned over an electrochemically active feature in HOPG, a Hg disc-well UME responded to activation of the substrate towards K^+ uptake. HOPG CVs confirmed the process under investigation was K^+ intercalation/deintercalation and not plating/stripping. However, the complex electrochemical response observed on the substrate electrode at potentials where the SEI is expected to form was chemically resolved by the probe, which did not identify a significant steady-state flux of K^+ towards the interface until potentials well into the expected intercalation range.

We compared the activity towards K⁺ intercalation on two structurally different sites on the HOPG surface. Despite contrast in their Raman signatures, indicating a different degree of disorder, and differences in their redox reactivity as assessed by the use of the feedback mode of SECM, few differences were detected on their K⁺ flux activity. While HOPG is likely not a top candidate for KIBs, the new capabilities brought by these probes make them of interest to further understand the role of heterogeneities on ion insertion mechanisms in energy materials. Hg disc-well UMEs can acquire localized, chemically specific measurements of ionic flux over operating battery electrode materials. This information is inaccessible to existing analytical methods and will help inform the rational design of future alkali ion battery anodes and cathodes. CV-SECM imaging studies of multiple alkali ion intercalation and de-intercalation processes at target energy storage materials are in progress and planned for future publications.

Funding

This material is based upon work supported by the National Science Foundation under Grant No. DMR-1611268 and the National Science Foundation Graduate Research Fellowship Program under Grant No. DGE-1144245. Any opinions, findings, and conclusions or recommendations expressed in this material are those of the authors and do not necessarily reflect the views of the National Science Foundation. J.R.-L. acknowledges support from an Alfred P. Sloan Foundation Fellowship. The authors also thank UIUC for generous start-up funds.

Acknowledgements

Sample characterization were carried out in part in the Frederick Seitz Materials Research Laboratory Central Facilities, University of Illinois. Sample preparation was carried out in part in the Micro and Nanotechnology Laboratory, University of Illinois. The authors thank Dr. Kenneth Hernández-Burgos for assistance with editing.

Appendix A. Supplementary data

Supplementary data associated with this article can be found in the online version at http://dx.doi.org/10.1016/j.electacta.2017. 04.105.

References

- [1] V. Etacheri, R. Marom, R. Elazari, G. Salitra, D. Aurbach, Challenges in the development of advanced Li-ion batteries: a review, Energy Environ. Sci. 4 (2011) 3243–3262, doi:http://dx.doi.org/10.1039/c1ee01598b.
- [2] H. Vikström, S. Davidsson, M. Höök, Lithium availability and future production outlooks, Appl. Energy. 110 (2013) 252–266, doi:http://dx.doi.org/10.1016/j. apenergy.2013.04.005.
- [3] D. Larcher, J.M. Tarascon, Towards greener and more sustainable batteries for electrical energy storage, Nat. Chem. 7 (2014) 19–29, doi:http://dx.doi.org/ 10.1038/nchem.2085.
- [4] S.R. Taylor, Abundance of chemical elements in the continental crust: a new table, Geochim. Cosmochim. Acta. 28 (1964) 1273–1285, doi:http://dx.doi.org/ 10.1016/0016-7037(64)90129-2.
- [5] L. Xue, Y. Li, H. Gao, W. Zhou, X. Lü, W. Kaveevivitchai, A. Manthiram, J.B. Goodenough, Low-Cost High-Energy Potassium Cathode, J. Amer. Chem. Soc. 139 (2017) 2164–2167, doi:http://dx.doi.org/10.1021/jacs.6b12598.
- [6] A.J. Bard, L.R. Faulkner, Electrochemical Methods: Fundamentals and Applications, 2nd ed, Wiley, New York, 2001.
- [7] C. Vaalma, G.A. Giffin, D. Buchholz, S. Passerini, Non-Aqueous K-Ion Battery Based on Layered K_{0.3}MnO₂ and Hard Carbon/Carbon Black, J. Electrochem. Soc. 163 (2016) A1295–A1299, doi:http://dx.doi.org/10.1149/2.0921607jes.
- [8] Z. Jian, Z. Xing, C. Bommier, Z. Li, X. Ji, Hard Carbon Microspheres: Potassium-Ion Anode Versus Sodium-Ion Anode, Adv. Energy Mater. 6 (2015) 1501874– 1501875, doi:http://dx.doi.org/10.1002/aenm.201501874.
- [9] Z. Jian, W. Luo, X. Ji, Carbon Electrodes for K-lon Batteries, J. Am. Chem. Soc. 137 (2015) 11566–11569, doi:http://dx.doi.org/10.1021/jacs.5b06809.

- [10] W. Luo, J. Wan, B. Ozdemir, W. Bao, Y. Chen, J. Dai, H. Lin, Y. Xu, F. Gu, V. Barone, L. Hu, Potassium Ion Batteries with Graphitic Materials, Nano Lett. 15 (2015) 7671–7677, doi:http://dx.doi.org/10.1021/acs.nanolett.5b03667.
- [11] K. Share, A.P. Cohn, R. Carter, B. Rogers, C.L. Pint, Role of Nitrogen-Doped Graphene for Improved High-Capacity Potassium Ion Battery Anodes, ACS Nano. 10 (2016) 9738–9744, doi:http://dx.doi.org/10.1021/acsnano.6b05998.
- [12] Z.J. Barton, J. Rodríguez-López, Lithium Ion Quantification Using Mercury Amalgams as in Situ Electrochemical Probes in Nonaqueous Media, Anal. Chem. 86 (2014) 10660–10667, doi:http://dx.doi.org/10.1021/ac502517b.
- [13] J. Hui, M. Burgess, J. Zhang, J. Rodríguez-López, Layer Number Dependence of Li⁺ Intercalation on Few-Layer Graphene and Electrochemical Imaging of Its Solid-Electrolyte Interphase Evolution, ACS Nano 10 (2016) 4248–4257, doi: http://dx.doi.org/10.1021/acsnano.5b07692.
- [14] E. Ventosa, W. Schuhmann, Scanning electrochemical microscopy of Li-ion batteries, Phys. Chem. Chem. Phys. 17 (2015) 28441–28450, doi:http://dx.doi.org/10.1039/C5CP02268A.
- [15] P. Schwager, H. Bülter, I. Plettenberg, G. Wittstock, Review of Local InSitu Probing Techniques for the Interfaces of Lithium-Ion and Lithium-Oxygen Batteries, Energy Technol. 4 (2016) 1472–1485, doi:http://dx.doi.org/10.1002/ ente.201600141.
- [16] Z.J. Barton, J. Rodríguez-López, Emerging scanning probe approaches to the measurement of ionic reactivity at energy storage materials, Anal. Bioanal. Chem. 408 (2016) 2707–2715, doi:http://dx.doi.org/10.1007/s00216-016-9373-7.
- [17] L. Danis, S.M. Gateman, C. Kuss, S.B. Schougaard, J. Mauzeroll, Nanoscale Measurements of Lithium-Ion-Battery Materials using Scanning Probe Techniques, ChemElectroChem 4 (2016) 6–19, doi:http://dx.doi.org/10.1002/ celc.201600571.
- [18] Z.J. Barton, J. Rodríguez-López, Cyclic Voltammetry Probe Approach Curves with Alkali Amalgams at Mercury Sphere-Cap Scanning Electrochemical Microscopy Probes, Anal. Chem. 89 (2017) 2708–2715, doi:http://dx.doi.org/ 10.1021/acs.analchem.6b04093.
- [19] J. Velmurugan, M.V. Mirkin, Fabrication of Nanoelectrodes and Metal Clusters by Electrodeposition, ChemPhysChem 11 (2010) 3011–3017, doi:http://dx.doi. org/10.1002/cphc.201000321.
- [20] L. Danis, D. Polcari, A. Kwan, S.M. Gateman, J. Mauzeroll, Fabrication of Carbon, Gold, Platinum, Silver, and Mercury Ultramicroelectrodes with Controlled Geometry, Anal. Chem. 87 (2015) 2565–2569, doi:http://dx.doi.org/10.1021/ac503767n.
- [21] Z.J. Barton, J. Rodríguez-López, Fabrication and Demonstration of Mercury Disc-Well Probes for Stripping-Based Cyclic Voltammetry Scanning Electrochemical Microscopy, Anal. Chem. 89 (2017) 2716–2723, doi:http://dx. doi.org/10.1021/acs.analchem.6b04022.
- [22] G.J. Hills, L.M. Peter, Electrode kinetics in aprotic media, J. Electroanal. Chem. Interfacial Electrochem. 50 (1974) 175–185, doi:http://dx.doi.org/10.1016/ S0022-0728(74)80149-X.
- [23] M.T.M. Koper, W. Schmickler, A theory for amalgam forming electrode reactions, J. Electroanal. Chem. 450 (1998) 83–94, doi:http://dx.doi.org/ 10.1016/S0022-0728(97)00474-9.
- [24] M. Burgess, K. Hernández-Burgos, K.J. Cheng, J.S. Moore, J. Rodríguez-López, Impact of electrolyte composition on the reactivity of a redox active polymer studied through surface interrogation and ion-sensitive scanning electrochemical microscopy, Analyst 141 (2016) 3842–3850, doi:http://dx.doi. org/10.1039/C6AN00203J.
- [25] A.C. Ferrari, J. Robertson, Interpretation of Raman spectra of disordered and amorphous carbon, Phys. Rev. B 61 (2000) 14095–14107, doi:http://dx.doi.org/ 10.1103/PhysRevB.61.14095.
- [26] Y. Yamada, K. Miyazaki, T. Abe, Role of Edge Orientation in Kinetics of Electrochemical Intercalation of Lithium-Ion at Graphite, Langmuir 26 (2010) 14990–14994, doi:http://dx.doi.org/10.1021/la1019857.
- [27] D. Aurbach, Review of selected electrode-solution interactions which determine the performance of Li and Li ion batteries, J. Power Sources 89 (2000) 206–218, doi:http://dx.doi.org/10.1016/S0378-7753(00)00431-6.
- [28] N.S. Norberg, S.F. Lux, R. Kostecki, Interfacial side-reactions at a LiNi_{0.5}Mn_{1.5}O₄ electrode in organic carbonate-based electrolytes, Electrochem. Commun. 34 (2013) 29–32, doi:http://dx.doi.org/10.1016/j.elecom.2013.04.007.
- [29] S. Kuss, D. Trinh, L. Danis, J. Mauzeroll, High-Speed Scanning Electrochemical Microscopy Method for Substrate Kinetic Determination: Method and Theory, Anal. Chem. 87 (2015) 8096–8101, doi:http://dx.doi.org/10.1021/acs. analchem.5b01268.
- [30] A.N. Patel, M.G. Collignon, M.A. O'Connell, W.O.Y. Hung, K. McKelvey, J.V. Macpherson, P.R. Urwin, A New View of Electrochemistry at Highly Oriented Pyrolytic Graphite, J. Am. Chem. Soc. 134 (2012) 20117–20130, doi:http://dx.doi.org/10.1021/ja308615h.
- [31] N. Nioradze, R. Chen, N. Kurapati, A. Khvataeva-Domanov, S. Mabic, S. Amemiya, Organic Contamination of Highly Oriented Pyrolytic Graphite As Studied by Scanning Electrochemical Microscopy, Anal. Chem. 87 (2015) 4836–4843, doi:http://dx.doi.org/10.1021/acs.analchem.5b00213.
- [32] C. Tan, J. Rodríguez-López, J.J. Parks, N.L. Ritzert, D.C. Ralph, S. Abercrombie, Reactivity of Monolayer Chemical Vapor Deposited Graphene Imperfections Studied Using Scanning Electrochemical Microscopy, ACS Nano 6 (2012) 3070– 3079, doi:http://dx.doi.org/10.1021/nn204746n.
- [33] J.-H. Zhong, J. Zhang, X. Jin, J.-Y. Liu, Q. Li, M.-H. Li, W. Cai, D.-Y. Wu, D. Zhan, B. Ren, Quantitative Correlation between Defect Density and Heterogeneous Electron Transfer Rate of Single Layer Graphene, J. Am. Chem. Soc. 136 (2014) 16609–16617, doi:http://dx.doi.org/10.1021/ja508965w.

- [34] P.R. Unwin, A.G. Güell, G. Zhang, Nanoscale Electrochemistry of sp² Carbon Materials: From Graphite and Graphene to Carbon Nanotubes, Acc. Chem. Res. 49 (2016) 2041–2048, doi:http://dx.doi.org/10.1021/acs.accounts.6b00301.
- [35] J. Hui, X. Zhou, R. Bhargava, A. Chinderle, J. Zhang, J. Rodríguez-López, Kinetic Modulation of Outer-Sphere Electron Transfer Reactions on Graphene Electrode with a Sub-surface Metal Substrate, Electrochim. Acta 211 (2016) 1016–1023, doi:http://dx.doi.org/10.1016/j.electacta.2016.06.134.
- [36] A. Molina, J. González, M.C. Henstridge, R.G. Compton, Analytical expressions for transient diffusion layer thicknesses at non uniformly accessible electrodes, Electrochim. Acta 56 (2011) 4589–4594, doi:http://dx.doi.org/ 10.1016/j.electacta.2011.02.085.
- [37] D. Trinh, E. Maisonhaute, V. Vivier, Electrical cross-talk in transient mode of scanning electrochemical microscopy, Electrochem. Commun. 16 (2012) 49–52, doi:http://dx.doi.org/10.1016/j.elecom.2012.01.003.
- [38] H. Kim, G. Yoon, K. Lim, K. Kang, A comparative study of graphite electrodes using the co-intercalation phenomenon for rechargeable Li, Na and K batteries, Chem. Commun. 52 (2016) 12618–12621, doi:http://dx.doi.org/10.1039/ C6CC05362A.
- [39] G.-C. Ri, C.-J. Yu, J.-S. Kim, S.-N. Hong, U.-G. Jong, M.-H. Ri, First-principles study of ternary graphite compounds cointercalated with alkali atoms (Li, Na, and K) and alkylamines towards alkali ion battery applications, J. Power Sources 324 (2016) 758–765, doi:http://dx.doi.org/10.1016/j.jpowsour.2016.05.136.
- [40] A.P. Cohn, N. Muralidharan, R. Carter, K. Share, L. Oakes, C.L. Pint, Durable potassium ion battery electrodes from high-rate cointercalation into graphitic carbons, J. Mater. Chem. A 4 (2016) 14954–14959, doi:http://dx.doi.org/ 10.1039/C6TA06797B.